Breaking new ground: *MB*ene route towards selective vinyl double bond hydrogenation in nitroarenes

Gourab Bhaskar,[1] Ranjan K. Behera,[1] Volodymyr Gvozdetskyi,[1#] Scott L. Carnahan,[1,2,3] Raquel A. Ribeiro,[4] Paul Oftedahl,[1] Charles Ward,[1] Paul C. Canfield,[2,4] Aaron J. Rossini,[1,2] Wenyu Huang, [1,2] Julia V. Zaikina[1*]

[1] *Department of Chemistry, Iowa State University, Ames, Iowa 50011, United States*

[2] *Ames Laboratory, US DOE, Iowa State University, Ames, Iowa 50011, United States*

[3] *Department of Chemistry, Saint Mary's University of Minnesota, Winona, Minnesota 55987, United States)*

[4] *Department of Physics and Astronomy, Iowa State University, Ames, Iowa 50011, United States*

[*] E-mail: yzaikina@iastate.edu

[#] Present Address: Department of Chemistry, University of Alberta, Edmonton, Alberta, Canada T6G 2G2.

Abstract. Doping, or incremental substitution of one element for another, is an effective way to tailor a compound's structure, as well as its physical and chemical properties. Herein, we replaced up to 30% of Ni with Co in members of the family of layered LiNiB compounds, stabilizing the high-temperature polymorph of LiNiB while the room-temperature polymorph does not form. By studying this layered boride with in-situ high-temperature powder diffraction, we obtained a distorted variant of $LiNi_{0.7}Co_{0.3}B$ featuring a perfect interlayer placement of $[Ni_{0.7}Co_{0.3}B]$ layers on top of each other – a structural motif not seen before in other borides. Because of the Co doping, $LiNi_{0.7}Co_{0.3}B$ can undergo a nearly complete topochemical Li deintercalation under ambient conditions, resulting in a metastable boride with formula $Li_{0.04}Ni_{0.7}Co_{0.3}B$. Heating of $Li_{0.04}Ni_{0.7}Co_{0.3}B$ in anaerobic conditions led to yet another metastable boride, $Li_{0.01}Ni_{0.7}Co_{0.3}B$, with a CoB-type crystal structure that cannot be obtained by simple annealing of Ni, Co, and B. No significant alterations of magnetic properties were detected upon Co-doping in the temperature-independent paramagnet $LiNi_{0.7}Co_{0.3}B$ or its Li-deintercalated counterparts. Finally, $Li_{0.01}Ni_{0.7}Co_{0.3}B$ stands out as an exceptional catalyst for the selective hydrogenation of the vinyl C=C bond in 3-nitrostyrene, even in the presence of other

competing functional groups. This research showcases an innovative approach to heterogeneous catalyst design by meticulously synthesizing metastable compounds.

Keywords: lithium, cobalt, boron, doping, ternary boride, solid-state NMR, PDF, *MB*ene, heterogeneous catalysis, metastable, hydrogenation, nitrobenzene.

Introduction

Layered compounds are of interest to the materials science community due to their versatile structural tunability and diverse properties [1-3]. Extensive research on graphene [4] laid the groundwork for developing materials beyond graphene [5]. Recent advancements in germanane, transition metal dichalcogenides, and 2D carbides – *MX*enes – have made the exploration of 2D materials even more relevant [6-14]. The 2D *MX*enes are formed upon topochemical deintercalation of loosely bonded '*A*' atoms from 3D layered $M_{n+1}AX_n$ phases (*MAX*), where *M* = an early transition metal, *A* = an element of group 13-14, and *X* = C or N [11-14]. As *MX*enes possess unique properties, the boron analogs of *MX*enes – *M*Benes – are a promising research topic. *M*Benes have been theoretically predicted to have applications as electrocatalysts, energy storage materials, and magnetic devices [15-23]; thus far, there are only a few examples of the bulk preparation of *M*Bene reported to date [21-23]. We have recently reported two layered polymorphs: *RT*-LiNiB and *HT*-LiNiB (*RT*- room temperature; *HT*- high temperature), featuring [NiB] layers alternating with loosely bonded Li layers [24]. Owing to the layered structures, we then studied the partial topochemical deintercalation of Li from the LiNiB layered polymorphs, leading to new metastable borides *RT*-$Li_{0.6}$NiB and *HT*-$Li_{0.4}$NiB [25]. Furthermore, we have shown that the [NiB] layers are quite flexible with respect to subtle changes in Li content and temperature, resulting in the two additional layered polymorphs, *RT*-Li_{1+x}NiB and *HT*-Li_{1+y}NiB [26].

To further fine-tune the topology and electronic structure of the [NiB] layers in the family of layered LiNiB compounds, we explored the effect of doping with other transition metals. Doping can tailor the crystal and electronic structures of a material, altering its magnetic and transport properties, absorption energy, and stability, thus enabling superior materials for catalysis, energy conversion, and storage. Borides of non-noble metals have been studied as catalysts for electrocatalytic water splitting and nitrogen reduction reactions owing to their stability and tunability of electronic structure [27-30]. While such studies tend to focus on nanomaterials based on binary transition metal borides [27-28, 30-31], ternary bulk borides have recently emerged as stable and active electrocatalysts [32-36]. Amorphous transition metal borides prepared *in situ* via a reaction of borohydride and transition metal (typically Ni) salts are well-known catalysts for hydrogenation [37]. Developing a heterogeneous catalyst that, in addition to its high selectivity and activity, does not contain noble metals is highly desirable for a

range of industrial processes. For example, the selective hydrogenation of nitroarenes is used to produce pharmaceuticals, fine chemicals, perfumes, polymers, and herbicides [38-39]. In the presence of more than one competing reducible functional group (such as $-NO_2$ and C=C in the case of 3-nitrostyrene), catalysts containing noble metals (Pt, Pd, Ru) simultaneously reduce both functional groups, resulting in limited selectivity [40-43]. Selective hydrogenation of the nitro ($-NO_2$) group in nitroarenes is a well-studied reaction and can be achieved by using a broad range of specially designed catalysts, including those that contain no noble metals [38-45]. On the other hand, only a few examples of selective hydrogenation of the vinyl (C=C) group in nitroarenes are reported; all utilize noble-metal-containing catalysts [46-49]. The selective hydrogenation of the C=C bond in 3-nitrostyrene over the nitro group enables the production of 3-nitroethylbenzene, a valuable intermediate to create more complex molecules for pharmaceuticals, agrochemicals, and other specialty chemicals. While 3-aminostyrene is the most produced product of 3-nitrostyrene hydrogenation, it is crucial to understand the catalytic systems in which the unconventional hydrogenation of C=C is preferred over the $-NO_2$ group from a fundamental research standpoint.

In this study, we characterize the interplay between crystal structures, magnetic and catalytic properties in the Li-Ni-Co-B compounds obtained via Co doping of layered LiNiB. The incorporation of Co changes the energy landscape, resulting in structural motifs not seen in the Li-Ni-B ternary system without considerably impacting magnetic properties. We further showed that the boride obtained upon Li deintercalation from the layered Li-Ni-Co-B compound demonstrates excellent conversion and selectivity towards the production of 3-ethylnitrobenzene via selective hydrogenation of vinyl (C=C) bond in 3-nitrostyrene.

Experimental. Co-doped LiNiB was synthesized via a high-temperature reaction of LiH, Ni, Co, and B powders, using the same procedure as the synthesis of *HT*-LiNiB and *HT*-$Li_{1+y}NiB$ compounds, but without quenching [24, 26]. For the topochemical deintercalation of Li to synthesize $Li_{0.04}Ni_{0.7}Co_{0.3}B$, 0.3-gram samples were exposed to air in a glass Petri dish for 10 days at room temperature, followed by washing with water and ethanol and drying under vacuum. At this point, PXRD measurements were made to ensure that the diffraction peak with the highest intensity (~20° 2θ, Cu $K\alpha$) in the PXRD pattern of Co-doped LiNiB had vanished completely. To synthesize $Li_{0.01}Ni_{0.7}Co_{0.3}B$ with the CoB-like structure, 0.15 g samples of $Li_{0.04}Ni_{0.7}Co_{0.3}B$ powder sealed in Nb tubes by arc melting in an argon-filled glovebox and slowly (1.56 K/min) heated from room temperature to 773 K, held at that temperature for 12 hours, and quenched in cold water. All samples were characterized via laboratory powder X-ray diffraction (PXRD) using a Rigaku MiniFlex600 powder diffractometer with Cu Kα radiation (λ = 1.54051 Å). The elemental analysis was performed via energy-dispersive X-ray spectroscopy (EDXS) and inductively coupled plasma mass spectrometry (ICP-MS). Solid state ^{7}Li and ^{11}B NMR spectra were measured on a Bruker widebore 9.4 T (400 MHz) NMR spectrometer equipped with an Avance III HD console. A 2.5 mm probe and a 25 kHz magic angle spinning frequency were used in all cases. Room-temperature high-resolution synchrotron powder diffraction and total scattering data suitable for PDF analysis were collected at beamline 11-BM (λ = 0.45784 Å) and 11-ID-B (λ = 0.14320 Å), respectively, at Advanced Photon Source Argonne National Laboratory (APS ANL). *In situ* high-temperature synchrotron powder X-ray diffraction data were collected at 17-BM (APS ANL) in the temperature range 298-1200 K and an average wavelength λ = 0.24158 Å. Magnetic property measurements were done on the polycrystalline samples using Quantum Design MPMS XL and MPMS3 SQUID magnetometers. Prior to performing catalytic measurements, freshly washed and dried samples (except arc-melted "$Ni_{0.7}Co_{0.3}B$") were ball-milled in polystyrene grinding vials with slip-on caps using a SPEX SamplePrep 8000M Mixer/Mill for 6 minutes in air. Liquid phase hydrogenation of 3-nitrostyrene was performed according to a literature method [49] with small modifications. The reaction mixture was diluted and analyzed by an Agilent 6890N/5975 gas chromatograph-mass spectrometer (GC-MS) equipped with an HP-5ms capillary column and a flame ionization detector (FID). Further details of synthesis and characterization methods used can be found in the Supporting Information.

Results and Discussion

1. Family of ternary layered polymorphs in the Li-Ni-B system.

The hydride synthesis route used here replaces ductile Li metal with a powdered LiH precursor, allowing for the intimate mixing of starting materials, exceptional compositional control, lower synthesis temperature, and faster reaction time than the traditional solid state synthesis route [50-53]. The hydride route led to the discovery of a family of ternary layered polymorphs (Figure S1) *RT*-LiNiB, *HT*-LiNiB, *RT*-$Li_{1+x}NiB$, and *HT*-$Li_{1+y}NiB$ (where *RT* and *HT* stand respectively for room temperature and high temperature) with unique layered structural motif of alternating single-atom-thick Li and [NiB] layers. Exposing Li-enriched *RT*-$Li_{1+x}NiB$ and *HT*-$Li_{1+y}NiB$ polymorphs to air first rapidly transforms these phases to their Li-depleted descendants *RT*-LiNiB and *HT*-LiNiB. Upon prolonged exposure to air, the latter compounds convert into novel layered borides *RT*-$Li_{0.6}NiB$ and *HT*-$Li_{0.4}NiB$ [25], whose structures consist of randomly-distributed atomically-ordered substructures $Li[NiB]_n$ (n = 1, 2, 3). Upon further heating in a sealed niobium container, *HT*-$Li_{0.4}NiB$ transforms into another novel metastable boride: $LiNi_{12}B_8$ [54], the synthesis of which is sensitive to slight changes in dwelling temperature and annealing time. Magnetic property measurements revealed that the 4 parent compounds (*RT*-LiNiB, *HT*-LiNiB, *RT*-$Li_{1+x}NiB$, and *HT*-$Li_{1+y}NiB$) are temperature-independent paramagnets, while the 3 metastable borides *RT*-$Li_{0.6}NiB$, *HT*-$Li_{0.4}NiB$ and $LiNi_{12}B_8$ exhibit spin-glass like behavior at low temperatures [24-26, 54]. Therefore, we were interested in how the substitution of Ni for Co affects the topology of the [NiB] layers, electronic structure, and resulting magnetic properties. Substitution of Ni with other 3*d* metals was attempted but could not be achieved in $LiNi_{1-x}T_xB$ for *T* = Mn, Fe, Cu.

2. Incorporation of Co in the [NiB] layers of LiNiB.

To synthesize Co-doped LiNiB, we followed the same temperature profile as was used for *RT*-LiNiB and *RT*-$Li_{1+x}NiB$ [28, 30]. Surprisingly, in the presence of Co, *HT*-type, and *HT*(1+y)-type compounds were stabilized instead of the *RT*-type phases. The highest yield of the target phases was achieved when the following experimentally determined starting molar ratios were used: LiH:Ni:Co:B = 1.3:(1-x):x:1.15 for the *HT*-type phase and LiH:Ni:Co:B = 1.4:(1-x):x:1.15 for *HT*-(1+y)-type phase. Throughout this text, the terminology *HT*-type and *HT*-(1+y)-type phase has been used to signify that the PXRD patterns of the $LiNi_{1-x}Co_xB$ compounds match the PXRD patterns of *HT*-LiNiB [24] or *HT*-$Li_{1+y}NiB$ [26], respectively. The 30% excess of LiH and

15% excess of B powder are required for the phase pure samples, as in the synthesis of other lithium nickel borides [24, 26]. An additional excess of LiH is required to stabilize the *HT*-(1+y)-type phase in line with its Li-rich composition compared to the *HT*-type phase. Our previous reports indicate that to stabilize both *HT*-LiNiB and *HT*-$Li_{1+y}NiB$, the samples need to be quenched in cold water from 1173 K [24, 26]. Therefore, Co doping stabilizes compounds whose PXRD patterns resemble those of *HT*-LiNiB and *HT*-$Li_{1+y}NiB$ without the need for quenching (Figure 1, S2). This suggests that the Co atoms are incorporated in the [NiB] layer and that Co incorporation has the same effect as heating to higher temperatures.

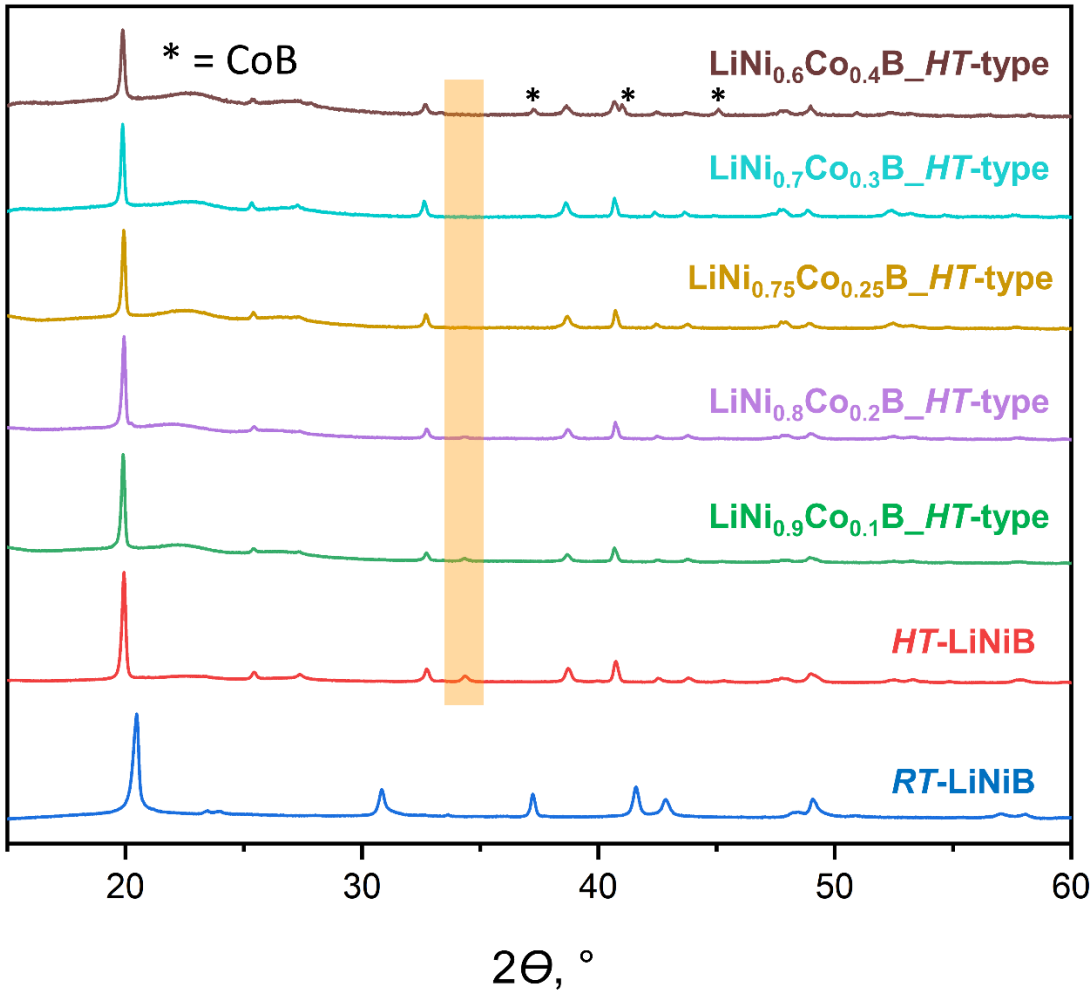

Figure 1. PXRD patterns (Cu K_α wavelength) of $LiNi_{1-x}Co_xB$ resemble those of *HT*-LiNiB but not *RT*-LiNiB. The highlighted region shows a change in the PXRD patterns with increasing Co-content, implying the incorporation of Co within the LiNiB structure.

Analysis of the PXRD data reveals variation in the position and intensity of diffraction peaks (Figure 1, S2; highlighted region) with increasing Co content from x = 0.1 to x = 0.3 in the $LiNi_{1-x}Co_xB$ compounds. The absence of diffraction peaks for Co metal or any other known Co-containing compounds for x up to 0.3 suggests successful Co incorporation into the [NiB] layer. However, when the Co content increases to x= 0.4, diffraction peaks for the binary CoB phase are detected, indicating the substitution limit of Co to be near x = 0.3 for both *HT*-type and *HT*(1+y)-type $LiNi_{1-x}Co_xB$ compounds (Figure 1, S2).

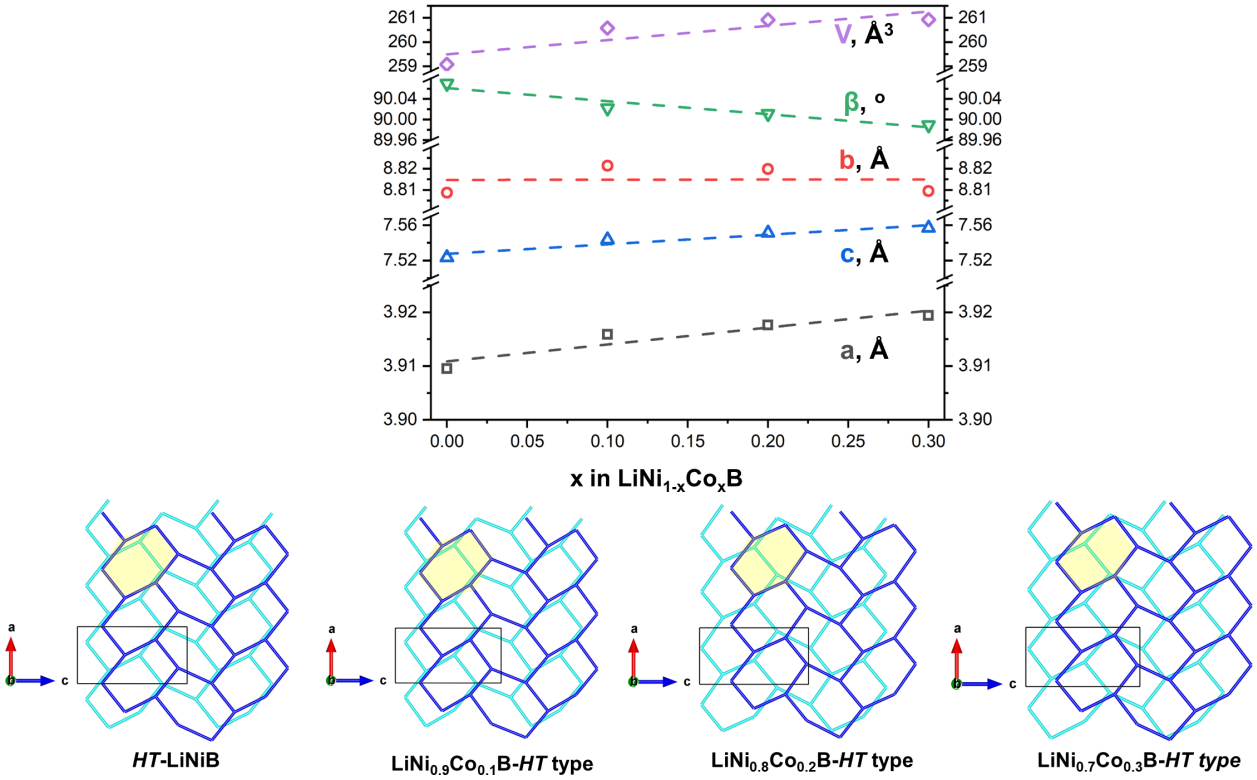

Figure 2. Variation of the unit cell parameters and volume with Co content, x, in $LiNi_{1-x}Co_xB$. The dashed lines represent a linear fit, and the error bars are smaller than the symbols used. Increasing Co content leads to a relative interlayer shift of the *MB*ene layers in *HT*-type $LiNi_{1-x}Co_xB$. Only Ni/Co layers are shown, and Li and B atoms are omitted for clarity. The dark-blue layer represents the top Ni/Co layer, and the light-blue layer represents the bottom Ni/Co layer. The distorted Ni_6 hexagon is highlighted in yellow to emphasize the relative shift of Ni/Co interlayers with an increment of Co content.

The variation in the PXRD patterns with the increment of Co content is a result of the incorporation of Co within the [NiB] layer. Unit cell parameters of *HT*-type and *HT*(1+y)-type

$LiNi_{1-x}Co_xB$ compounds with variable Co-content (x = 0.1, 0.2, 0.3) were determined via Rietveld refinement of high-resolution synchrotron PXRD data using *HT*-LiNiB and *HT*(1+y)-LiNiB as a structure model (Table S1). Gradual changes in the unit cell parameters (*a*, *b*, *c*, *β*, and *V*) with increasing Co content for both *HT*-type and *HT*(1+y)-type $LiNi_{1-x}Co_xB$ compounds are in agreement with the larger atomic size of Co compared to Ni. A relative interlayer shift between the top and bottom *MB*ene layers (highlighted in Figure 2 with yellow shading) was detected for the *HT*-type $LiNi_{1-x}Co_xB$ with variation in x. On the other hand, a considerable decrease in the *β* angle (highlighted in Figure S3), approaching 90°, was found for the *HT*(1+y)-type $LiNi_{1-x}Co_xB$ without a significant shift of the *MB*ene layers. These gradual changes in the crystal structures of solid solutions in both *HT*-type and *HT*(1+y)-type $LiNi_{1-x}Co_xB$ compounds with the variation of the Co content evidence the incorporation of Co within the [NiB] layer.

Scanning electron microscopy (SEM) for *HT*-type and *HT*(1+y)-type $LiNi_{0.7}Co_{0.3}B$ further confirms uniform Ni/Co distribution and reveals the crystallite morphology (Figure S4). The false-colored backscattered electron images show that Co and Ni atoms are uniformly distributed throughout the scanned region, confirming Co incorporation within the LiNiB structure. Both compounds feature plate-like particle morphologies similar to those of *RT*-LiNiB and *HT*-LiNiB. Energy-dispersive X-ray analysis (EDX) verifies the presence of three elements, Ni, Co, and B, even though an accurate quantification of Li and B cannot be achieved due to the limitations of the EDX method with light elements. Signals for Ta/Nb (material of the tube used for synthesis) or any other heavy elements besides Ni and Co were not detected in the samples. The experimental Ni/Co ratios of 2.3(1) and 2.3(4) were determined via the EDX method by averaging the Ni and Co at. % for 4 and 7 areas in *HT*-type and *HT*(1+y)-type $LiNi_{0.7}Co_{0.3}B$ samples, respectively. The determined Ni/Co ratios agree well with the expected ratio of 2.33 in $LiNi_{0.7}Co_{0.3}B$.

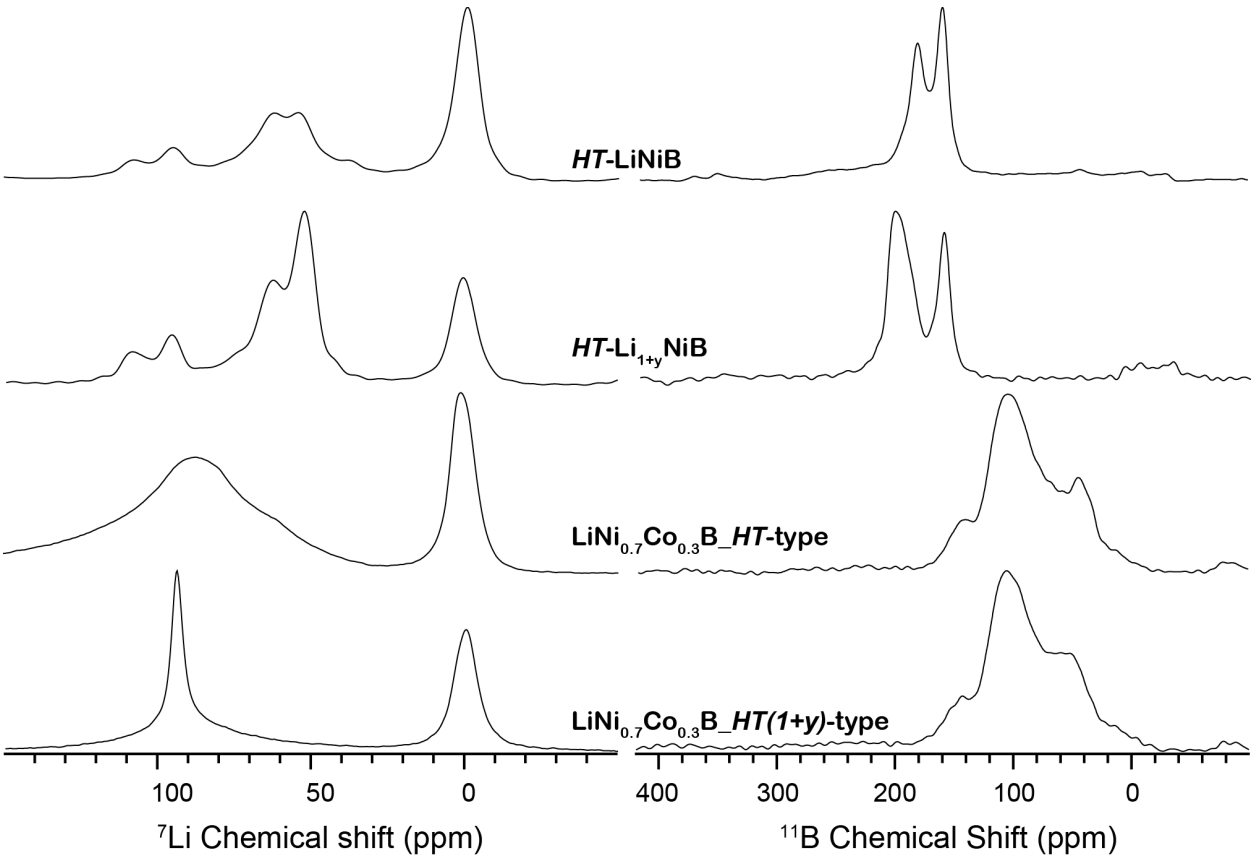

Figure 3. ^{7}Li and ^{11}B MAS solid-state NMR spectra of *HT*-type and *HT*(1+y)-type $LiNi_{0.7}Co_{0.3}B$ compounds in comparison to *HT*-LiNiB, and *HT*-$Li_{1+y}NiB$. The differences in the peak positions and intensities are consistent with the alteration of the Li and B environments in these compounds due to the incorporation of Co within the [NiB] layer.

After confirmation of Co incorporation into the LiNiB structure, we collected solid-state magic angle spinning (MAS) ^{7}Li and ^{11}B NMR data to determine how the Li and B environments change upon Co doping (Figure 3). The ^{7}Li and ^{11}B NMR spectra of *HT*-type and *HT*(1+y)-type $LiNi_{0.7}Co_{0.3}B$ compounds clearly differ from those of *HT*-LiNiB and *HT*-$Li_{1+y}NiB$, respectively. The changes in the Li and B coordination environment shown by the NMR spectra provide another piece of evidence for Co incorporation into the structure of LiNiB. The peak at 0 ppm in the ^{7}Li NMR spectra of *HT*-type and *HT*(1+y)-type $LiNi_{0.7}Co_{0.3}B$ compounds corresponds to the impurity phase $LiOH{\cdot}H_2O$ or Li_2O. The ^{7}Li and ^{11}B NMR chemical shifts are in the typical range for metallic compounds, with similar chemical shifts observed for *RT*-LiNiB, *HT*-LiNiB, *RT*-$Li_{1+x}NiB$, and *HT*-$Li_{1+y}NiB$ [24, 26].

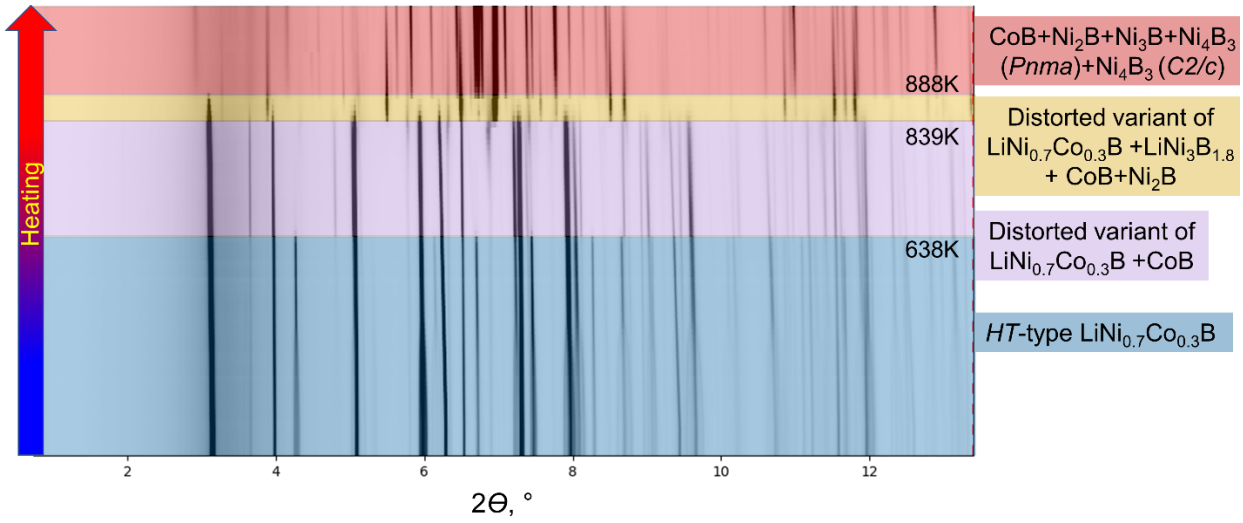

Figure 4. *In situ* high-temperature synchrotron powder X-ray diffraction data (wavelength λ = 0.24158 Å) of *HT*-type $LiNi_{0.7}Co_{0.3}B$ shows gradual leaching of Li due to the reaction of Li with the silica capillary. Increasing temperature causes the transformation sequence *HT*-type $LiNi_{0.7}Co_{0.3}B$ → distorted variant of $LiNi_{0.7}Co_{0.3}B$ → $LiNi_3B_{1.8}$ → CoB, Ni_2B, Ni_3B, and Ni_4B_3.

High-temperature synchrotron PXRD data were collected to study possible transformations of the layered *HT*-type and *HT*(1+y)-type $LiNi_{0.7}Co_{0.3}B$ compounds upon heating (Figure 4, S5-S7). Heating of *HT*(1+y)-type $LiNi_{0.7}Co_{0.3}B$ in a silica capillary first transforms it into the *HT*-type $LiNi_{0.7}Co_{0.3}B$ compound (Figure S6: 506 K), confirming the presence of extra Li atoms in the *HT*(1+y)-type $LiNi_{0.7}Co_{0.3}B$. Further heating resulted in a PXRD pattern that is similar to but different from that of both *HT*-type and *HT*(1+y)-type $LiNi_{0.7}Co_{0.3}B$ compounds, suggesting considerable structural distortion of the *MB*ene layers (Figure 4: 638 K, Figure S6: 793 K). These PXRD data were refined in the *Pnma* structural model (Figure S8, Table S2, see the experimental section in SI for details about refinement), where the *MB*ene layers stack perfectly on top of each other. Such stacking has never been observed in other layered members of the LiNiB family of compounds [24-26] (Figure S9, 5). With further temperature increase, *HT*-type and *HT*(1+y)-type $LiNi_{0.7}Co_{0.3}B$ compounds first transform to $LiNi_3B_{1.8}$ and finally to CoB and binary borides of nickel Ni_2B, Ni_3B, and Ni_4B_3 (Figure 4: 888 K, Figure S6: 1029 K, Figures S5, S7). We presume that Li is gradually "leached" from the structure (due to the side reaction with silica), stabilizing Li-depleted compounds upon heating. PXRD patterns for both *HT*-type and *HT*(1+y)-type $LiNi_{0.7}Co_{0.3}B$ compounds at room temperature did not reveal any known Co-

containing compounds. Still, the appearance of CoB peaks at higher temperatures again suggests that Co was first incorporated into the LiNiB structure and then transformed into CoB once the layered structure collapsed upon heating.

We have recently investigated the flexibility of the [NiB] layers with respect to subtle changes in composition and temperature [26]. A slight increase in Li content on going from *HT*-LiNiB to *HT*-$Li_{1+y}NiB$ led to a relative shift between two adjacent [NiB] layers, altering their stacking order and resulting in a change in space group from $P2_1/m$ to $P2_1/c$ [26]. On the other hand, an increase in temperature (≥616 K) upon *in situ* heating of *HT*-LiNiB resulted in a distorted variant of the polymorph (refined in the same $P2_1/m$ space group) that features deformed Ni_6 units with a relative shift of [NiB] layers (Figure 5) [30]. Herein, we increase the complexity even more and explore the flexibility of [NiB] layers with respect to electron count (Co-doping) as well as temperature (*in situ* heating of Co-doped samples). We observed that the effect of Co doping is similar to that of temperature since Co doping induces a substantial change in [NiB] layers, resulting in the *HT*-polymorph with no quenching from high temperatures needed, as opposed to the expected *RT*-polymorph. The transition from the *RT* to *HT*-type driven by both Co-doping and quenching from high temperature most likely occurs due to the comparable energies of these layered polymorphs. The variation in synthesis temperature (quenching/no quenching), electronic (number of valence electrons), and size effects between Ni and Co, alter the energy landscape and stabilize the *HT*-type phase. An analogy can be drawn to the monoborides of 3*d*-transition metals *T*B (where *T* = V, Cr, Mn, Fe, Co), whose structure bears some similarities with the [NiB] layers found in LiNiB polymorphs. As the number of valence electrons and the size of the metal atom vary from V to Co, the structure changes from the CrB-type for VB to the FeB-type for CoB. However, MnB and FeB have both high-temperature FeB-type and low-temperature CrB-type polymorphs and can also form peculiar intergrowths of both CrB- and FeB- fragments when synthesized at lower temperatures. Similar cases of polymorphism are seen in other intermetallic compounds [55-57].

Furthermore, Co doping causes a relative interlayer shift of $[Ni_{1-x}Co_xB]$ layers with an increment of Co-content in *HT*-type $LiNi_{1-x}Co_xB$ ($P2_1/m$), similar to the structural change induced by temperature in *HT*-LiNiB [30] (Figure 2, 5). *In situ* heating of the *HT*-type $LiNi_{0.7}Co_{0.3}B$ compound (≥638 K) stabilized a distorted variant of $LiNi_{0.7}Co_{0.3}B$, which features the perfect placement of $[Ni_{1-x}Co_xB]$ layers on top of each other (*Pnma* space group), that has

never been seen in LiNiB compounds (Figure S8, 5). Therefore, we conclude that all three parameters – Li "chemical" pressure due to variation in Li content, synthesis temperature, and valence electron concentration within the [$Ni_{1-x}Co_xB$] layer affect the topology, relative shift, and, therefore, the stacking order of the [$Ni_{1-x}Co_xB$] layers. Clearly, this family of layered LiNiB structures that can tolerate variation in composition, electron count, and temperature is an example of remarkable structural flexibility.

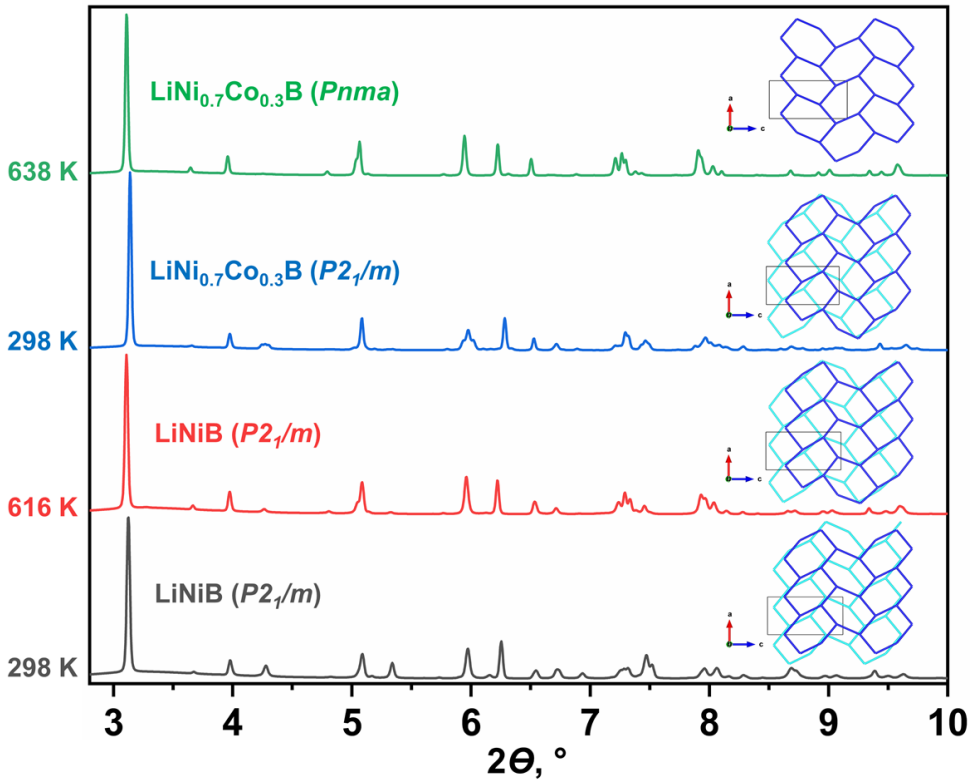

Figure 5. Relative shift of *MB*ene layers in the structures of *HT*-LiNiB [28], *HT*-LiNiB at 616 K [30], *HT*-type $LiNi_{0.7}Co_{0.3}B$, and the distorted variant of *HT*-type $LiNi_{0.7}Co_{0.3}B$ at 638 K as determined from *in situ* PXRD synchrotron data (wavelength $\lambda = 0.24158$ Å).

3. Topochemical deintercalation of Li.

Exploiting the unique layered topology with loosely bonded Li atoms, we recently synthesized two novel metastable borides, *RT*-$Li_{0.6}NiB$ and *HT*-$Li_{0.4}NiB$, upon partial topochemical deintercalation of Li from *RT*- and *HT*-LiNiB [25]. Since the layered structural motif is preserved in both the *HT*-type and *HT*(1+y)-type $LiNi_{0.7}Co_{0.3}B$ compounds, we investigated the effect of Co-doping on the Li-deintercalation. Both *HT*-type and *HT*(1+y)-type

$LiNi_{0.7}Co_{0.3}B$ were exposed to air for a prolonged period of time. Similar to the *HT*-$Li_{1+y}NiB$ case, initial exposure of the *HT*(1+y)-type $LiNi_{0.7}Co_{0.3}B$ compound to air transforms it first to the *HT*-type $LiNi_{0.7}Co_{0.3}B$ phase, and with longer time in air sample becomes semicrystalline (Figure S10). The transformation of *HT*(1+y)-type $LiNi_{0.7}Co_{0.3}B$ to *HT*-type $LiNi_{0.7}Co_{0.3}B$ in air again confirms the presence of extra Li atoms in the *HT*(1+y)-type $LiNi_{0.7}Co_{0.3}B$. The loss of crystallinity upon exposure of *HT*-type $LiNi_{0.7}Co_{0.3}B$ to the air for 10 days, taken together with the basic pH of the solution obtained upon washing the sample with deionized water (due to the formation of LiOH), confirms the fact that Li is deintercalated from the layers (Figure S10). To quantitatively estimate the amount of Li deintercalated from the *HT*-type $LiNi_{0.7}Co_{0.3}B$ compound, the Li/Ni/Co ratio was determined with inductively coupled plasma mass spectrometry (ICP-MS). ICP-MS data indicate that ~96% of Li atoms have been deintercalated from the *HT*-type $LiNi_{0.7}Co_{0.3}B$ compound, resulting in the composition $Li_{0.039(7)}Ni_{0.73(1)}Co_{0.23(1)}B$. The Co-content from the ICP-MS data is slightly less (0.23 vs. 0.3) than the Co-loading content used in the synthesis of $LiNi_{0.7}Co_{0.3}B$.

To confirm the partial Li deintercalation and to track variation in the Li and B coordination environments upon deintercalation, solid-state ^{7}Li, and ^{11}B NMR spectra were acquired. Other than the presence of an impurity peak at ~0 ppm (for Li_2O, $LiOH{\cdot}H_2O$, or LiOH), the fact that there are still some broad peaks in the 0-100 ppm range in the ^{7}Li NMR spectra confirms the incomplete extent of the Li-deintercalation (Figure S11). Comparison of ^{7}Li and ^{11}B NMR spectra of $Li_{0.04}Ni_{0.7}Co_{0.3}B$ with those of *HT*-type and *HT*(1+y)-type $LiNi_{0.7}Co_{0.3}B$ and *HT*-$Li_{0.4}NiB$ highlight the differences in Li and B coordination environments due to the incorporation of Co within the LiNiB framework as well as due to the Li deintercalation.

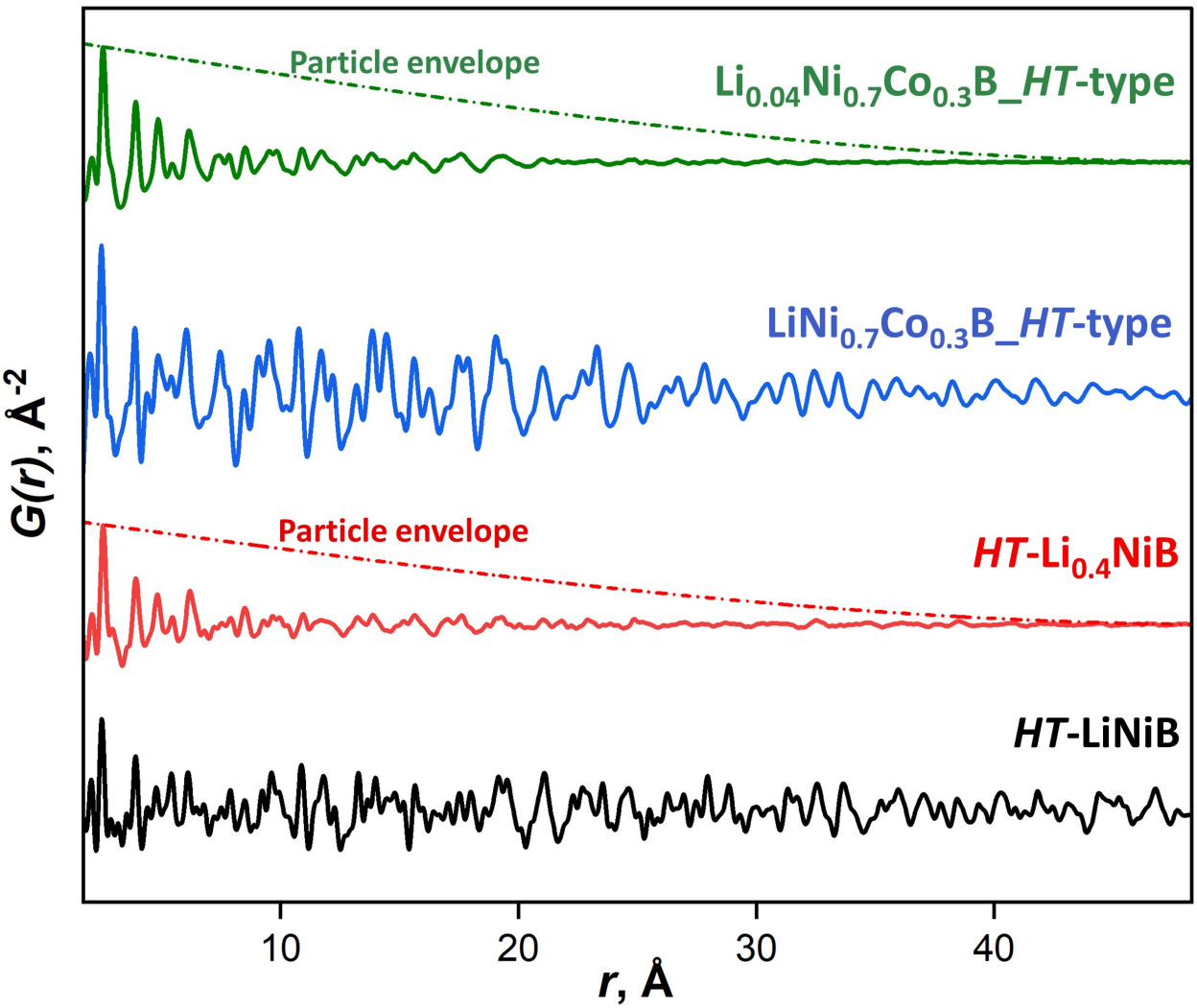

Figure 6. Pair distribution functions (PDF) of *HT*-LiNiB, *HT*-$Li_{0.4}NiB$, *HT*-type $LiNi_{0.7}Co_{0.3}B$, and $Li_{0.04}Ni_{0.7}Co_{0.3}B$ showing loss of crystallinity upon partial topochemical deintercalation of Li.

The dashed line denotes the particle envelope function $f_e(r,d) = \left[1 - \frac{3r}{2d} + \frac{1}{2}\left(\frac{r}{d}\right)^3\right]\theta(r,d)$, where d is particle diameter (equal to 50 Å for this fit) and θ is a step function of value 1 for $r < d$ and 0 otherwise.

Previously, complex crystal structures of *RT*-$Li_{0.6}NiB$ and *HT*-$Li_{0.4}NiB$ obtained by partial Li deintercalation from LiNiB polymorphs were solved by concurrently using STEM, DFT, and PDF data; therefore, PDF data were also acquired to determine the $Li_{0.04}Ni_{0.7}Co_{0.3}B$ structure. Comparing the PDF data for *HT*-type $LiNi_{0.7}Co_{0.3}B$ with its partially Li-deintercalated counterpart again confirmed loss of crystallinity upon partial topochemical Li-deintercalation

(Figure 6). However, fitting the PDF data of $Li_{0.04}Ni_{0.7}Co_{0.3}B$ with the previously established models based on a random intergrowth of three substructures *HT*-Li[NiB]$_n$ (n =1, 2, 3) [25] did not produce a sufficiently good fit. This indicates that the structure of $Li_{0.04}Ni_{0.7}Co_{0.3}B$ (with 96% of Li deintercalated) is sufficiently different from that of *HT*-$Li_{0.4}NiB$ (with 60% of Li deintercalated), consistent with the ICP-MS data suggesting that more Li was deintercalated from the Co-doped compound. We hypothesize that increasing the Co content causes a relative shift of the Ni/Co interlayers, which reduces the overall stability of the layered structure and ultimately facilitates more complete Li deintercalation under mild conditions.

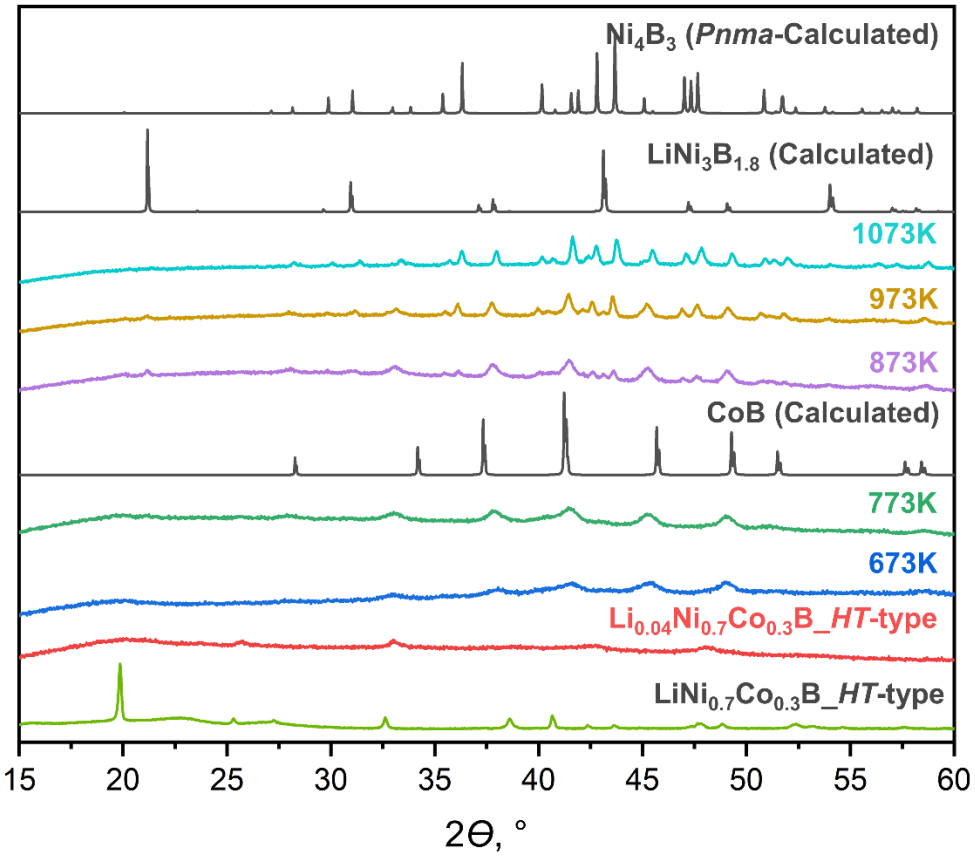

Figure 7. PXRD patterns (Cu K_α wavelength) of compounds resulting from *ex-situ* heat treatment of $Li_{0.04}Ni_{0.7}Co_{0.3}B$ at different temperatures after a 12-hour dwelling time. Calculated PXRD patterns of CoB [ICSD-30450], $LiNi_3B_{1.8}$ [ICSD-111367], and Ni_4B_3 [ICSD-24307] have been added for reference.

4. Ex-situ heating of the $Li_{0.04}Ni_{0.7}Co_{0.3}B$ compound.

As was recently reported, a novel $LiNi_{12}B_8$ compound forms upon heating the *HT*-$Li_{0.4}NiB$ phase obtained via Li deintercalation from *HT*-LiNiB [54]. We then attempted to study how the structure of $Li_{0.04}Ni_{0.7}Co_{0.3}B$ (obtained by Li deintercalation of *HT*-type $LiNi_{0.7}Co_{0.3}B$) changes with heating and whether it is possible to obtain Co-doped $LiNi_{12}B_8$. For the *ex-situ* heat treatment, the $Li_{0.04}Ni_{0.7}Co_{0.3}B$ sample was sealed in a niobium tube, and heated at different temperatures for 12 hours, and cooled quickly by quenching (Figure 7). Upon heating at 673 K and 773 K for 12 hours, the sample becomes more crystalline, but the overall change in the PXRD pattern indicates severe reorganization of $[Ni_{1-x}Co_xB]$ layers. Further heating leads to a minor fraction of $LiNi_3B_{1.8}$, and at the highest temperature of 1073 K, the formation of Ni_4B_3 and CoB is observed (Figure 7, S12). Therefore, unlike heating the *HT*-$Li_{0.4}NiB$ phase at 973 K for 12h, which led to the $LiNi_{12}B_8$ compound, no such compound could be detected upon heating $Li_{0.04}Ni_{0.7}Co_{0.3}B$. This result indicates that the incorporation of Co within the LiNiB structure hinders the formation of a $LiNi_{12}B_8$-type phase. Additionally, this could signify that Co-doping increases the extent of Li-deintercalation possible, resulting in a compound with a Li:Co ratio too small to favor the formation of a $LiNi_{12}B_8$-type phase.

A comparison of the PXRD patterns for the samples quenched from 673 K and 773 K with the calculated PXRD pattern of CoB [ICSD-30450] revealed a striking resemblance. CoB and NiB crystallize in two different orthorhombic structures: CoB (FeB structure type, *Pbnm*, a = 3.948 Å, b = 5.243 Å, c = 3.037 Å, V = 62.86 Å^3, Z = 4, ICSD-30450) and NiB (CrB structure type, *Cmcm*, a = 2.925 Å, b = 7.396 Å, c = 2.966 Å, V = 64.16 Å^3, Z = 4, ICSD-26937) (Figure S13). The CoB structure resembles the [NiB] layer in *HT*-LiNiB, although the CoB structure is not layered (Figure S13). Therefore, the question about the structure and stability of the NiB-CoB solid solution arises. The PXRD pattern of the sample obtained upon *ex-situ* heating of the Ni-rich $Li_{0.04}Ni_{0.7}Co_{0.3}B$ compound at 773 K matches well with the CoB but not the NiB structure. To confirm this, the Le-Bail fitting of the PXRD pattern of the sample quenched at 773 K with the CoB structure provided an excellent fit, suggesting the formation of a NiB-CoB solid solution with the CoB structure type (Figure S14). Comparison of the refined unit cell parameters obtained from the Le-Bail fitting of the PXRD pattern with the reported unit cell parameters for CoB [ICSD-30450] indicated an increase in a and b and a decrease in c unit cell parameters, resulting in an overall increase in unit cell volume (Table S3). The excellent fit of

the X-ray PDF data for the $Li_{0.04}Ni_{0.7}Co_{0.3}B$ sample quenched at 773 K using the CoB structural model [ICSD-30450] confirmed that the obtained Ni-rich boride crystallizes in the CoB structure type (Figure 8a). This boride is likely a metastable phase since an attempt to arc-melt elemental powders of composition "$Ni_{0.7}Co_{0.3}B$" resulted in phase segregation to a mixture of NiB and CoB (Figure S15). According to the respective binary phase diagrams, CoB melts congruently near 1450°C, whereas NiB decomposes incongruently near 1035°C, so the formation of a NiB-CoB solid solution by crystallization from a high-temperature melt is unlikely.

The solid-state MAS ^{7}Li NMR spectra (Figure S16) indicated that the CoB-type "$Ni_{0.7}Co_{0.3}B$" sample still contains some Li atoms. The Li/Ni/Co ratio obtained using ICP-MS suggests that the composition is $Li_{0.011(8)}Ni_{0.76(3)}Co_{0.23(2)}B$. The experimental Ni/Co ratio of 2.37(9) determined from EDX data by averaging the Ni/Co ratio in 7 areas of the sample agrees well with the expected Ni/Co ratio of 2.33 in the *HT*-type $LiNi_{0.7}Co_{0.3}B$ precursor. Even though the CoB structural model provided a good fit of the X-ray PDF and PXRD data, the ~1% Li from ICP-MS and qualitative data from MAS ^{7}Li NMR data suggest minor doping of Li into Ni/Co sites. Mixing of Li and Ni in the same crystallographic sites has also been observed in another compound in the Li-Ni-B system—$LiNi_{12}B_8$. In that case, in addition to two fully occupied Li sites, 5 Li/Ni mixed occupied sites were confirmed by solid-state ^{7}Li-NMR [54]. Mixing of Li sites with other transition metals, particularly with Mn, Co, and Ni, was also observed in layered oxide cathodes for lithium-ion batteries [58].

As evidenced from SEM images, CoB-type $Li_{0.01}Ni_{0.7}Co_{0.3}B$ features a plate-like bulk morphology (Figure 8b), most likely inheriting it from the layered Li-containing precursor (*HT*-type $LiNi_{0.7}Co_{0.3}B$) used for synthesis even though the CoB structure itself is not layered (Figure S13).

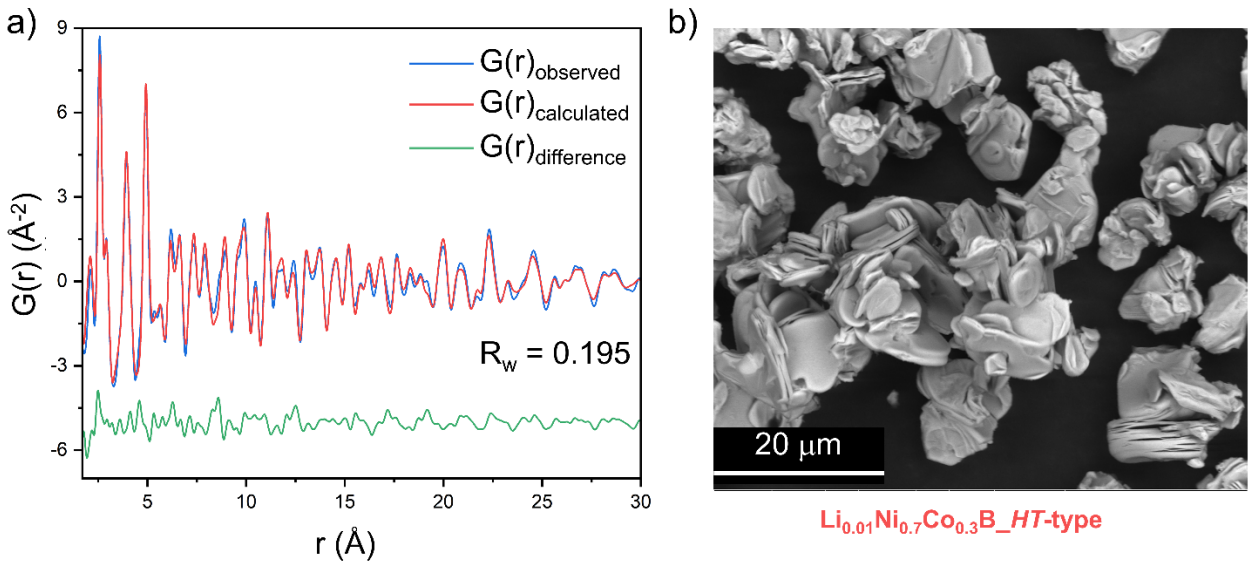

Figure 8. a) Fitting of the X-ray PDF data of $Li_{0.04}Ni_{0.7}Co_{0.3}B$ sample obtained via *ex-situ* heating at 773 K with the CoB structural model; b) backscattered electron (BSE) image of $Li_{0.01}Ni_{0.7}Co_{0.3}B$ showing a plate-like bulk morphology.

5. Magnetic properties.

First, we compare the magnetic properties of compounds in the LiNiB family with their Co-containing counterparts. All four parent layered compounds: *RT*-LiNiB, *HT*-LiNiB, *RT*-$Li_{1+x}NiB$, and *HT*-$Li_{1+y}NiB$, are temperature-independent (Pauli) paramagnets [24, 26]. Temperature-independent molar magnetic susceptibility and a linear dependence of magnetization on the applied field are consistent with temperature-independent (Pauli) paramagnetism for both the *HT*-type and *HT*(1+y)-type $LiNi_{0.7}Co_{0.3}B$ compounds (Figure S17). Such behavior is identical to their ternary analogs *HT*-LiNiB and *HT*-$Li_{1+y}NiB$; therefore, no alteration of magnetic properties upon Co doping into Ni sites in LiNiB occurs.

We then compare the magnetic properties of Li-deintercalated *RT*-$Li_{0.6}NiB$, *HT*-$Li_{0.4}NiB$, and $LiNi_{12}B_8$ [54] with their Co-containing analogs (Figure 9, Figure S18-S20). A spin glass-like state below 30 K was revealed in all 3 metastable borides: *RT*-$Li_{0.6}NiB$, *HT*-$Li_{0.4}NiB$ [25], and $LiNi_{12}B_8$, the latter of which is obtained upon heating of *HT*-$Li_{0.4}NiB$ [54]. On the other hand, NiB and CoB were reported to be non-moment-bearing compounds (weakly paramagnetic/diamagnetic) [59-60].

$Li_{0.04}Ni_{0.7}Co_{0.3}B$ obtained via deintercalation displays paramagnetic behavior below 100 K, a Curie Weiss tail upon cooling, ZFC/FC splitting in *M/H*(*T*) data in low field (50 Oe), and an *S*-

shaped $M(H)$ curve at 2K, suggesting a low-temperature magnetic transition, although the small magnetic moment per transition metal rebuts bulk magnetism (Figure S19). $Li_{0.01}Ni_{0.7}Co_{0.3}B$ with CoB-structure (Figure 9 and Figure S19-20) exhibits similar behavior. We corrected data for a trace amount of ferromagnetic impurity using the Honda-Owen method [61-62] and obtained intrinsic $M/H(T)$ that was fitted with the modified Curie-Weiss equation, $\chi = \chi_0 + C/(T - \Theta)$ (Table S4, Figure 9, Figure S19). Such analysis yielded an effective moment of 0.1-0.2 μ_B per transition metal in $Li_{0.01}Ni_{0.7}Co_{0.3}B$, which is comparable to the effective moment per Ni atom in other Li-Ni-B compounds with a spin glass-like state below 30 K [25, 54]. On the other hand, the contribution of the temperature-independent term (χ_0) in the case of $Li_{0.01}Ni_{0.7}Co_{0.3}B$ is negligible, while the Weiss constant, Θ, approaches 0. In summary, the magnetic properties of $Li_{0.04}Ni_{0.7}Co_{0.3}B$ and $Li_{0.01}Ni_{0.7}Co_{0.3}B$ with a CoB-like structure differ from non-moment bearing CoB and NiB and resemble those of *HT*-$Li_{0.4}NiB$ with a potential low-temperature magnetic transition and a small effective moment per transition metal [25]. Co-doping does not induce significant magnetic coupling in LiNiB compounds or their Li-deintercalated derivatives.

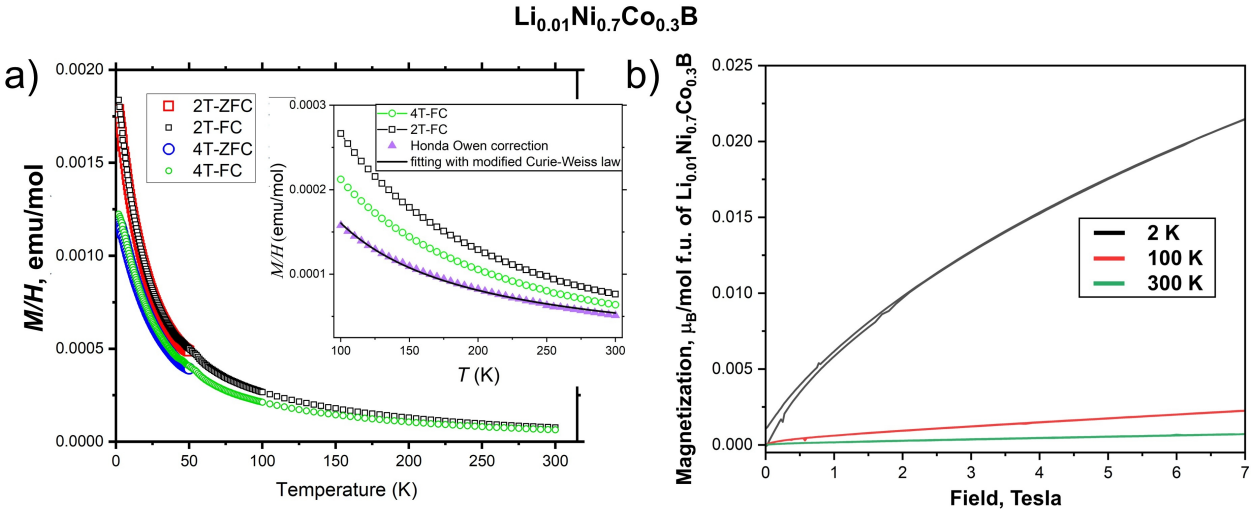

Figure 9. a) Temperature-dependent ZFC/FC molar $M/H(T)$ for $Li_{0.01}Ni_{0.7}Co_{0.3}B$ in the 2-300 K temperature range measured under an applied field of 2 T and 4 T; inset: the Honda-Owen method was used to obtain intrinsic $M/H(T)$ for $Li_{0.01}Ni_{0.7}Co_{0.3}B$, which was then fitted using the modified Curie-Weiss law (see Table S4 for fitting parameters) in the 100-300 K temperature range; (b) field-dependent magnetization at 2K, 100K and 300 K for $Li_{0.01}Ni_{0.7}Co_{0.3}B$.

Considering the layered morphology of Ni-rich metastable $Li_{0.01}Ni_{0.7}Co_{0.3}B$ with a CoB-like structure, we investigated the catalytic hydrogenation activity of this compound.

6. Liquid-Phase Hydrogenation of 3-nitrostyrene.

The design of efficient heterogeneous catalysts for selective hydrogenation of vinyl (C=C) groups is critical for the industrial production of fine chemicals. However, when a substrate molecule contains more than one reducible group, such as C=C and nitro -NO_2 moieties in nitrostyrenes, precious metal catalysts tend to reduce both groups simultaneously, resulting in limited selectivity [39-43]. Strategies to address the problem of chemoselectivity include modification of the active site of a catalyst with ligands, zeolites, and metal-organic frameworks [63-65]. In most of these cases, the intention is to block or passivate the catalytic surface such that production of the undesired product(s) is suppressed. The selectivity increase comes at the cost of a reduction in overall catalytic activity. Another approach to address the selectivity issues is metal doping, which can lead to a change in the adsorption mode and modulation of electron density of the substrate molecules on the catalyst surface [42, 66]. For example, the doping of Co into Ru active sites resulted in a compressed Ru lattice, thus enhancing the selectivity for hydrogenation of 4-nitrostyrene to 4-aminostyrene [66]. The majority of studies of the selective hydrogenation of nitrostyrene focus on nitro group hydrogenation to obtain amines [38-45, 66], while the examples of catalysts capable of selective vinyl C=C bond hydrogenation in nitrostyrenes are limited to Pt- and Pd-nanoparticles [46-49]. For instance, Rh-doped Pd nanocubes and a cellulose nanocrystal-supported Pd-Co bimetallic catalyst exhibit enhanced activity and selectivity for C=C in the presence of a nitro group due to the modulation of surface electron density and adsorption energy [47-48].

We studied the catalytic activity of $Li_{0.01}Ni_{0.7}Co_{0.3}B$ in the industrially relevant liquid phase hydrogenation of nitroarenes and compared its catalytic activity with CoB, *RT*-$Li_{0.6}NiB$ [25], *HT*-$Li_{0.4}NiB$ [25]. Here, $Li_{0.01}Ni_{0.7}Co_{0.3}B$ demonstrated >99% selectivity to the vinyl C=C hydrogenation product 3-ethylnitrobenzene from 3-nitrostyrene with 77.4% conversion over 12 hours of reaction at 100 °C. The formation of other competing products—3-aminostyrene and 3-ethylaniline—was not detected, emphasizing the superior selectivity of $Li_{0.01}Ni_{0.7}Co_{0.3}B$ in the liquid-phase hydrogenation of 3-nitrostyrene. As established previously, the $Li_{0.01}Ni_{0.7}Co_{0.3}B$ compound crystallizes in the CoB structure type. Therefore, to understand whether the catalytic activity stems from the presence of Co or due to the CoB structure type, we studied the catalytic activity of CoB for the same reaction. Phase-pure CoB was prepared via the hydride route

(Figure S21). Surprisingly, CoB did not show any activity in the hydrogenation reaction indicating that either the Ni metal or the layered morphology of $Li_{0.01}Ni_{0.7}Co_{0.3}B$ played a role in the catalysis. Hence, we investigated the catalytic activity of *RT*-$Li_{0.6}NiB$ and *HT*-$Li_{0.4}NiB$, which feature a layered morphology but are Co-free, as well as $Li_{0.04}Ni_{0.7}Co_{0.3}B$, which does not have the CoB structure. These compounds also did not exhibit any activity for the hydrogenation reaction. Therefore, we can conclude that the layered morphology, as well as the simultaneous presence of both Ni and Co, play a key role in the selective hydrogenation of the vinyl C=C bond in 3-nitrostyrene, even in the presence of another reducible functional group -NO_2. Furthermore, a sample prepared by arc-melting Ni, Co, and B (Figure S15) contains primarily CoB and NiB phases but no layered morphology and does not show appreciable catalytic activity. Therefore, the exceptional selectivity of $Li_{0.01}Ni_{0.7}Co_{0.3}B$ in selective hydrogenation of C=C in nitrostyrene manifests the interplay between composition, crystal, and electronic structure in this metastable boride and its catalytic activity. We note, however, that long-term (> 12 months) storage of this catalyst in air results in reduced conversion attributed to surface oxidation. After washing the sample with water and ethanol and drying under vacuum, the conversion was restored to >90%, but the catalyst became less selective. Further studies are needed to investigate the catalyst's surface using in-situ techniques. Ordered intermetallic compounds have been suggested as promising heterogeneous catalysts for hydrogeneration reactions [67-71], including noble-metal-free catalysts with exceptional activity [68, 69] and selective catalysts for -NO_2 group hydrogenation in nitroarenes [45]. Similarly, in electrocatalysis, multimetallic borides were shown to have great promise to reduce overpotential, resulting in catalysts with increased activity [32-36]. The metastable $Li_{0.01}Ni_{0.7}Co_{0.3}B$ discussed here manifests a CoB-type structure with atomic mixing of Ni, Co, and Li that most likely affords the surface configuration required for exceptional selectivity. While the structure of the surface and Co/Ni distribution remains the subject of ongoing studies, the current study illustrates a fruitful avenue for the design of heterogeneous catalysts: accessing unique electronic and crystal structures with tailored surfaces via the synthesis of metastable compounds.

Table 1. Catalytic performance of catalysts for chemoselective hydrogenation of 3-nitrostyrene.[a]

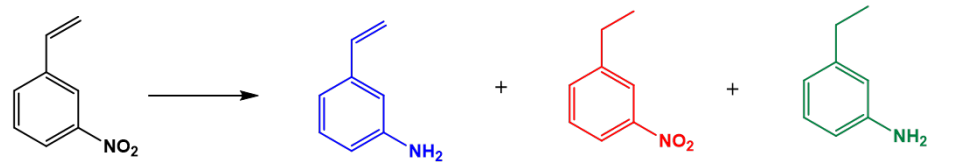

3-nitrostyrene (NS) 3-aminostyrene (AS) 3-ethylnitrobenzene (ENB) 3-ethylaniline (EA)

Entry	Catalyst(s)[a]	Conversion (%)	Selectivity (%)		
			AS	ENB	EA
1	No catalyst	0	-	-	-
2	CoB	0	-	-	-
3	*HT*-$Li_{0.4}NiB$	0	-	-	-
4	*RT*-$Li_{0.6}NiB$	0	-	-	-
5	$Li_{0.04}Ni_{0.7}Co_{0.3}B$	0	-	-	-
6	arc-melted $Ni_{0.7}Co_{0.3}B$	0	-	-	-
7	$Li_{0.01}Ni_{0.7}Co_{0.3}B$	77.4	-	>99	-
8	5% Pt/C	100	0.3	-	99.7

[a] Reaction conditions: 20 mg catalyst, 50 mg 3-nitrostyrene, 20 mg xylene, 2 mL toluene, 700 rpm, 100 °C, 12 h.

Conclusion

In this study, we demonstrated the successful doping of Co into the layered LiNiB compounds, stabilizing two solid solutions, *HT*-type and *HT*-(1+y)-type $LiNi_{1-x}Co_xB$ ($x \leq 0.3$). Substitution of Co for Ni was confirmed by PXRD, solid-state ^{7}Li and ^{11}B NMR spectroscopy, and EDX. We determined that up to 30% Co can be substituted into the [NiB] layers in LiNiB. *In situ* high-temperature synchrotron PXRD revealed the formation of a distorted variant of $LiNi_{0.7}Co_{0.3}B$ upon heating of *HT*-type and *HT*-(1+y)-type $LiNi_{0.7}Co_{0.3}B$ compounds. This high-temperature structure features precise alignment of [NiB] layers perpendicular to their stacking direction, not observed in other Li-Ni-B compounds. The topochemical deintercalation of Li in air stabilizes a novel metastable boride $Li_{0.04}Ni_{0.7}Co_{0.3}B$. Unlike the Li-deintercalation from ternary LiNiB phases where 40-60% Li can be removed, e.g., *HT*-$Li_{0.4}NiB$, ~96% Li can be deintercalated from the *HT*-type $LiNi_{0.7}Co_{0.3}B$ compound resulting in $Li_{0.04}Ni_{0.7}Co_{0.3}B$, as evidenced from ICP-MS data. *Ex-situ* heating $Li_{0.04}Ni_{0.7}Co_{0.3}B$ in a sealed niobium container led

to yet another novel metastable boride: $Li_{0.01}Ni_{0.7}Co_{0.3}B$. Excellent fitting of both the X-ray PDF and PXRD patterns with the CoB structure evidence that this Ni-rich compound crystallizes in the CoB structure type, which is different from the NiB structure type. Co-doping did not result in substantially different magnetic properties in *HT*-type and *HT*(1+y)-type $LiNi_{0.7}Co_{0.3}B$, which remain temperature-independent paramagnets, while $Li_{0.04}Ni_{0.7}Co_{0.3}B$ and $Li_{0.01}Ni_{0.7}Co_{0.3}B$ exhibit low-temperature magnetic transitions. Finally, the excellent selectivity of $Li_{0.01}Ni_{0.7}Co_{0.3}B$ in hydrogenating the vinyl (C=C) bond in 3-nitrostyrene yielding 3-ethylnitrobenzene as a single product distinguishes this metastable boride from the other heterogeneous catalysts.

Associated content.

Additional Tables with crystallographic data, Rietveld refinement plots, and structure comparisons can be found in the Supporting Information. This material is available free of charge via the Internet at http://pubs.acs.org.

Author information.

Corresponding Author

* yzaikina@iastate.edu

Notes: The authors declare no competing financial interest.

Acknowledgments. Financial support from the National Science Foundation (U.S.) Division of Materials Research (DMR-1944551) CAREER Award is gratefully acknowledged. R.K.B. and W.H. (catalysis and ICP-MS) were supported by National Science Foundation (CHE-2108306/2108307) and Trapp Innovation Award. A.J.R., S.L.C. (NMR spectroscopy), and P.C.C. (magnetism) were supported by the U.S. Department of Energy (DOE), Office of Science, Basic Energy Sciences, Materials Science and Engineering Division through the Ames National Laboratory. The Ames Laboratory is operated for the U.S. Department of Energy by Iowa State University under contract #DE-AC02-07CH11358. R.A.R. was supported by the Gordon and Betty Moore Foundation's EPiQS Initiative through Grant GBMF4411. Use of the Advanced Photon Source at Argonne National Laboratory was supported by the U. S. Department of Energy, Office of Science, Office of Basic Energy Sciences, under Contract No. DE-AC02-06CH11357. We thank Dr. Kirill Kovnir (Chemistry Department, Iowa State University and US-

DOE Ames Laboratory) for the access to PXRD and Aishwarya Mantravadi Chemistry Department, Iowa State University) for the help with SEM/EDXS data acquisition. The paper is adapted from the dissertation of Dr. Gourab Bhaskar.

References.

1. Rao, C. N. R.; Ramakrishna Matte, H. S. S.; Maitra, U. Graphene Analogues of Inorganic Layered Materials. *Angew. Chem. Int. Ed*. **2013**, *52*, 13162-13185.
2. Duong, D. L.; Yun, S. J.; Lee, Y. H. van der Waals Layered Materials: Opportunities and Challenges. *ACS Nano*. **2017**, *11*, 11803–11830.
3. Wang, X.; Sun, Y.; Liu, K. Chemical and structural stability of 2D layered materials. *2D Mater*. **2019**, *6*, 042001.
4. Novoselov, K. S.; Geim, A. K. The rise of graphene. *Nature Mater*. **2007**, *6*, 183–191.
5. Butler, S. Z.; Hollen, S. M.; Cao, L.; Cui, Y.; Gupta, J. A.; Gutiérrez, H. R.; Heinz, T. F.; Hong, S. S.; Huang, J.; Ismach, A. F.; Johnston-Halperin, E.; Kuno, M.; Plashnitsa, V. V.; Robinson, R. D.; Ruoff, R. S.; Salahuddin, S.; Shan, J.; Shi, L.; Spencer, M. G.; Terrones, M.; Windl, W.; Goldberger, J. E. Progress, Challenges, and Opportunities in Two-Dimensional Materials Beyond Graphene. *ACS Nano*. **2013**, *7*, 2898–2926.
6. Bianco, E.; Butler, S.; Jiang, S.; Restrepo, O. D.; Windl, W.; Goldberger, J. E. Stability and Exfoliation of Germanane: A Germanium Graphane Analogue. *ACS Nano*. **2013**, *7*, 4414–4421.
7. Sun, Y.; Terrones, M.; Schaak, R. E. Colloidal Nanostructures of Transition-Metal Dichalcogenides. *Accounts of Chemical Research*. **2021**, *54*, 1517-1527.
8. Manzeli, S.; Ovchinnikov, D.; Pasquier, D.; Yazyev, O. V.; Kis, A.; 2D transition metal dichalcogenides. *Nat Rev Mater*. **2017**, *2*, 17033.
9. Wang, R.; Yu, Y.; Zhou, S.; Li, H.; Wong, H.; Luo, Z.; Gan, L.; Zhai, T. Strategies on Phase Control in Transition Metal Dichalcogenides. *Adv. Funct. Mater*. **2018**, *28*, 1802473.
10. Pi, L.; Li, L.; Liu, K.; Zhang, Q.; Li, H.; Zhai, T. Recent Progress on 2D Noble-Transition-Metal Dichalcogenides. *Adv. Funct. Mater*. **2019**, *29*, 1904932.
11. Gogotsi, Y.; Anasori, B. The Rise of MXenes. *ACS Nano*. **2019**, *13*, 8491–8494.

12. Naguib, M.; Kurtoglu, M.; Presser, V.; Lu, J.; Niu, J.; Heon, M.; Hultman, L.; Gogotsi, Y.; Barsoum, M. W. Two-Dimensional Nanocrystals Produced by Exfoliation of Ti_3AlC_2. *Adv. Mater*. **2011**, *23*, 4248−4253.
13. Alhabeb, M.; Maleski, K.; Anasori, B.; Lelyukh, P.; Clark, L.; Sin, S.; Gogotsi, Y. Guidelines for synthesis and processing of two-dimensional titanium carbide ($Ti_3C_2T_x$ MXene). *Chem. Mater*. **2017**, *29*, 7633-7644.
14. Barsoum, M. W.; Eklund, P. The $M_{n+1}AX_n$ Phases: The Precursors for MXenes. In 2D Metal Carbides and Nitrides (MXenes), Structure, Properties and Applications; Springer: Cham, Switzerland, **2019,** 15-35.
15. Yang, X.; Shang, C.; Zhou, S.; Zhao, J. MBenes: emerging 2D materials as efficient electrocatalysts for the nitrogen reduction reaction. *Nanoscale Horiz*. **2020**, *5*, 1106-1115.
16. Khazaei, M.; Wang, J.; Estili, M.; Ranjbar, A.; Suehara, S.; Arai, S.; Esfarjani, K.; Yunoki, S. Novel MAB phases and insights into their exfoliation into 2D MBenes. *Nanoscale*. **2019**, *11*, 11305−11314.
17. Wang, Y.; Ma, N.; Liang, B.; Fan, J. Exploring the potential of Ti_2BT_2 (T = F, Cl, Br, I, O, S, Se and Te) monolayers as anode materials for lithium and sodium ion batteries. *Appl. Surf. Sci*. **2022**, *596*, 153619.
18. Jiang, Z.; Wang, P.; Jiang, X.; Zhao, J. MBene (MnB): a new type of 2D metallic ferromagnet with high Curie temperature. *Nanoscale Horiz*. **2018**, *3*, 335−341.
19. Bo, T.; Liu, P. F.; Zhang, J.; Wang, F.; Wang, B.T. Tetragonal and trigonal Mo_2B_2 monolayers: two new low-dimensional materials for Li-ion and Na-ion batteries. *Phys. Chem. Chem. Phys*. **2019**, *21*, 5178–5188.
20. Guo, Z.; Zhou, J.; Sun, Z. New two-dimensional transition metal borides for Li ion batteries and electrocatalysis. *J. Mater. Chem. A*. **2017**, *5*, 23530−23535.
21. Zhou, J.; Palisaitis, J.; Halim, J.; Dahlqvist, M.; Tao, Q.; Persson, I.; Hultman, L.; Persson, P. O. Å.; Rosen, J. Boridene: Two-dimensional $Mo_{4/3}B_{2-x}$ with ordered metal vacancies obtained by chemical exfoliation. *Science* **2021**, 373, 6556, 801-805.
22. Alameda, L. T.; Moradifar, P.; Metzger, Z. P.; Alem, N.; Schaak, R. E. Topochemical Deintercalation of Al from MoAlB: Stepwise Etching Pathway, Layered Intergrowth Structures, and Two-Dimensional MBene. *J. Am. Chem. Soc*. **2018**, *140*, 8833-8840.

23. Alameda, L. T.; Lord, R. W.; Barr, J. A.; Moradifar, P.; Metzger, Z. P; Steimle, B. C.; Holder, C. F.; Alem, N.; Sinnott, S. B.; Schaak, R. E. Multi-Step Topochemical Pathway to Metastable Mo_2AlB_2 and Related Two-Dimensional Nanosheet Heterostructures. *J. Am. Chem. Soc*. **2019**, *141*, 10852-10861.
24. Gvozdetskyi, V.; Bhaskar, G.; Batuk, M.; Zhao, X.; Wang, R.; Carnahan, S. L.; Hanrahan, M. P.; Ribeiro, R. A.; Canfield, P. C.; Rossini, A. J.; Wang, C. Z.; Ho, K. M.; Hadermann, J.; Zaikina, J. V. Computationally driven discovery of a family of layered LiNiB polymorphs. *Angew. Chem. Int. Ed*. **2019**, *131*, 16002-16009.
25. Bhaskar, G.; Gvozdetskyi, V.; Batuk, M.; Wiaderek, K.; Carnahan, S. L.; Sun, Y.; Wang, R.; Wu, X.; Zhang, C.; Ribeiro, R. A.; Bud'ko, S. L.; Canfield, P. C.; Rossini, A. J.; Huang, W.; Wang, C. Z.; Ho, K. M.; Hadermann, J.; Zaikina, J. V. Topochemical deintercalation of Li from layered LiNiB: toward 2D MBene. *J. Am. Chem. Soc*. **2021**, *143*, 4213–4223.
26. Gvozdetskyi, V.; Sun, Y.; Zhao, X.; Bhaskar, G.; Carnahan, S. L.; Harmer, C.; Zhang, F.; Ribeiro, R. A.; Canfield, P. C.; Rossini, A. J.; Wang, C. Z.; Ho, K. M.; Zaikina, J. V. Lithium Nickel Borides: evolution of *MB*ene layers driven by Li pressure. *Inorg. Chem. Front*. **2021**, *8*, 1675-1685.
27. Chen, H.; Zou, X. Intermetallic borides: structures, synthesis and applications in electrocatalysis. *Inorg. Chem. Front*. **2020**, *7*, 2248-2264.
28. Alexey, S.; Kovnir, K.; Shatruk, M.; Kolenko, Y. V. Critical Review of Platinum Group Metal-Free Materials for Water Electrolysis: Transition from the Laboratory to the Market: Earth-abundant borides and phosphides as catalysts for sustainable hydrogen production. *Johns. Matthey Technol. Rev*. **2021**, *65*, 207-226.
29. Fan, M.; Liang, X.; Li, Q.; Cui, L.; He, X.; Zou, X. Boron: A key functional component for designing high-performance heterogeneous catalysts. *Chin. Chem. Lett*. **2023**, 34, 107275.
30. Park, H.; Encinas, A.; Scheifers, J. P.; Zhang, Y.; Fokwa, B. P. T. Boron-Dependency of Molybdenum Boride Electrocatalysts for the Hydrogen Evolution Reaction. *Angew. Chem. Int. Ed.* **2017**, *56*, 5575.
31. Abeysinghe, J. P.; Kolln, A. F.; Gillan, E. G. Rapid and Energetic Solid-State Metathesis Reactions for Iron, Cobalt, and Nickel Boride Formation and Their Investigation as Bifunctional Water Splitting Electrocatalysts. *ACS Mater. Au*. **2022**, 2, 4, 489–504.

32. Rezaie, A. A.; Lee, E.; Yapo, J. A.; Fokwa, B. P. T. Highly Active and Abundant MAB Phases $Ni_{n+1}ZnB_n$ (n = 1, 2) toward Hydrogen Evolution. *Adv. Energy Sustainability Res*. **2021**, *2*, 2100052.
33. Mann, D.K.; Xu, J.; Mordvinova, N.E.; Yannello, V.; Ziouani, Y.; González-Ballesteros, N.; Sousa, J.P.S.; Lebedev, O.I.; Kolen'ko, Y.V.; Shatruk, M. Electrocatalytic water oxidation over $AlFe_2B_2$. *Chem. Sci*., **2019**, 10, 2796-2804.
34. Alameda, L.T.; Holder, C.F.; Fenton, J.L.; Schaak, R.E. Partial etching of Al from MoAlB single crystals to expose catalytically active basal planes for the hydrogen evolution reaction. *Chem. Mater.* **2017**, 29, 8953–8957.
35. Park, H.; Lee, E.; Lei, M.; Joo, H.; Coh, S.; Fokwa, B.P.T. Canonic-Like HER Activity of $Cr_{1-x}Mo_xB_2$ Solid Solution: Overpowering Pt/C at High Current Density. *Adv. Mater*. **2020**, 32, 2000855.
36. Fu, Y.; Richardson, P.; Li, K.; Yu, H.; Yu, B.; Donne, S.; Kisi, E.; Ma, T. Transition Metal Aluminum Boride as a New Candidate for Ambient-Condition Electrochemical Ammonia Synthesis. *Nano-Micro Lett*. **2020**, *12*, 65.
37. B. Ganem, B.; Osby, J. O. Synthetically Useful Reactions with Metal Boride and Aluminide Catalysts. *Chem. Rev*. **1986**, *86*, 763.
38. Formenti, D.; Ferretti, F.; Korbinian Scharnagl, F.; Beller, M. Reduction of Nitro Compounds Using 3d-Non-Noble Metal Catalysts. *Chem. Rev*. **2019**, 119, 2611-2680.
39. Blaser, H.-U.; Steiner, H.; Studer, M. Selective Catalytic Hydrogenation of Functionalized Nitroarenes: An Update. *ChemCatChem*, **2009**, 1, 210-221.
40. Boronat, M.; Concepción, P.; Corma, A.; González, S.; Illas, F.; Serna, P.; A Molecular Mechanism for the Chemoselective Hydrogenation of Substituted Nitroaromatics with Nanoparticles of Gold on TiO_2 Catalysts: A Cooperative Effect between Gold and the Support. *J. Am. Chem. Soc*. **2007**, 129, 16230–16237.
41. Corma, A.; Serna, P. Chemoselective Hydrogenation of Nitro Compounds with Supported Gold Catalysts. *Science* **2006**, 313, 332-334.
42. Peng, Y. H.; Geng, Z. G.; Zhao, S. T.; Wang, L. B.; Li, H. L.; Wang, X.; Zheng, X. S.; Zhu, J. F.; Li, Z. Y.; Si, R.; Zeng, J. Pt Single Atoms Embedded in the Surface of Ni Nanocrystals as Highly Active Catalysts for Selective Hydrogenation of Nitro Compounds. *Nano Lett*. **2018**, *18*, 3785-3791.

43. Serna, P.; Corma, A. Transforming Nano Metal Nonselective Particulates into Chemoselective Catalysts for Hydrogenation of Substituted Nitrobenzenes. *ACS Catal*. **2015**, 5, 7114–7121.
44. Corma, A.; Serna, P.; Concepción, P.; Calvino, J.J. Transforming Nonselective into Chemoselective Metal Catalysts for the Hydrogenation of Substituted Nitroaromatics. *J. Am. Chem. Soc.* **2008**, 130, 8748–8753.
45. Pei, Y.; Qi, Z.; Wei Goh, T.; Wang, L.-L.; Maligal-Ganesh, R. V.; MacMurdo, H. L.; Zhang, S.; Xiao, C.; Li, X.; Tao, F.; Johnson, D.D.; Huang, W.; Intermetallic structures with atomic precision for selective hydrogenation of nitroarenes. *J. of Catalysis* **2017**, 356, 307-314.
46. Beier, M.J.; Andanson, J.-M.; Baiker, A.; Tuning the Chemoselective Hydrogenation of Nitrostyrenes Catalyzed by Ionic Liquid-Supported Platinum Nanoparticles. *ACS Catal.* **2012**, 2, 2587–2595.
47. Wu, W.; Zhao, S; Cui, Y.E; Chen, W.; Liu, Y.; Wang, H.; Li, J.; Li, Z.; Zeng, J. Rh Doping in Pd Nanocubes Optimizes the Adsorption of 3-Nitrostyrene towards Selective Hydrogenation of Vinyl Group. *ChemCatChem* **2019**, 11, 2793-2798.
48. Li, X.; Zhu, X.; Ren, Z.; Si, X.; Lu, R.; Lu, F. Cellulose Nanocrystal-supported Pd-Co Bimetallic Catalyst for Selective Hydrogenation of 3-Nitrostyrene. ChemNanoMat. 2022, 8, e202200059.
49. Jiarui Zhao, J.; Fu, J. Wang, J.; Tang, K.; Liu, Q.; Huang, J. Particle-Size-Dependent Electronic Metal–Support Interaction in Pd/TiO_2 Catalysts for Selective Hydrogenation of 3-Nitrostyrene. *J. Phys. Chem. C* **2022**, 126, 15167–15174.
50. Adeyemi, A.; Bhaskar, G.; Cox, T.; Hong, S.; Gvozdetskyi, V.; Zaikina, J. V. Hydride Precursors in Materials Synthesis. *Comprehensive Inorganic Chemistry III*, Third Edition, *Elsevier,* **2023**.
51. Gvozdetskyi, V.; Hanrahan, M. P.; Ribeiro, R. A.; Kim, T.; Zhou, L.; Rossini, A. J.; Canfield P. C.; Zaikina, J. V. A hydride route to ternary alkali metal borides: a case study of lithium nickel borides. *Chem. Eur. J*. **2019**, *25*, 4123–4135.
52. Gvozdetskyi, V.; Owens-Baird, B.; Hong, S.; Cox, T.; Bhaskar, G.; Harmer, C.; Sun, Y.; Zhang, F.; Wang, C. Zh.; Ho, K. M.; Zaikina, J. V. From $NaZn_4Sb_3$ to *HT*-$Na_{1-x}Zn_{4-y}Sb_3$: Panoramic hydride synthesis, structural diversity, and thermoelectric properties. *Chem. Mater*. **2019**, *31*, 8695–8707.

53. Ma, X. C.; Xu, F.; Atkins, T. M.; Goforth, A. M.; Neiner, D.; Navrotsky, A.; Kauzlarich, S. M. A versatile low temperature synthetic route to Zintl phase precursors: Na_4Si_4, Na_4Ge_4 and K_4Ge_4 as examples. *Dalton Trans*. **2009**, 10250−10255.
54. Bhaskar, G.; Gvozdetskyi, V.; Carnahan, S. L.; Wang, R.; Mantravadi, A.; Wu, X.; Ribeiro, R. A.; Huang, W.; Rossini, A. J.; Ho, K. M.; Canfield, P. C.; Lebedev, O. I.; Zaikina, J. V. The path less traveled: a contemporary twist on synthesis and traditional structure solution of metastable $LiNi_{12}B_8$. *ACS Mater. Au*. **2022**, 2, 614–625.
55. Hohnke, D.; Parthé, E. *AB* Compounds with Sc, Y and Rare Earth Metals. II. FeB and CrB Type Structures of Monosilicides and Germanides. *Acta Cryst*. **1966,** 20, 572-582.
56. Klemenz, S.; Fries, M.; Dürrschnabel, M.; Skokov, K.; Kleebe, H.-J.; Gutfleisch, O.; Albert, B. Low-temperature synthesis of nanoscale ferromagnetic α′-MnB. *Dalton Trans*., **2020**, 49, 131-135.
57. Saldaña, F.I.; Defoy, E.; Janisch, D.; Rousse, G.; Autran, P.-O.; Ghoridi, A.; Séné, A.; Baron, M.; Suescun, L.; Le Godec, Y. Portehault, D. Revealing the Elusive Structure and Reactivity of Iron Boride α-FeB. *Inorg. Chem.* **2023**, *62*, 5, 2073–2082
58. Yan, P.; Zheng, J.; Lv, D.; Wei, Y.; Zheng, J.; Wang, Z.; Kuppan, S.; Yu, J.; Luo, L.; Edwards, D.; Olszta, M.; Amine, K.; Liu, J.; Xiao, J.; Pan, F.; Chen, G.; Zhang, J.-G.; Wang, C.-M. Atomic-Resolution Visualization of Distinctive Chemical Mixing Behavior of Ni, Co, and Mn with Li in Layered Lithium Transition-Metal Oxide Cathode Materials. *Chem. Mater*. **2015**, *27*, 5393–5401.
59. Buschow, K.H.J. (1977). Magnetic Properties of Borides. In: Matkovich, V.I. (eds) Boron and Refractory Borides. Springer, Berlin, Heidelberg.
60. Lundquist, N.; Myers, H. P.; Westin, R. The paramagnetic properties of the monoborides of V, Cr, Mn, Fe, Co and Ni. *Philos. Mag.* **1962**, *7*, 1187-1195.
61. Honda, K. Die thermomagnetischen Eigenschaften der Elemente. *Ann. Phys*. **1910**, 337, 1027-1063.
62. Owen, M. Magnetochemische Untersuchungen. Die thermomagnetischen Eigenschaften der Elemente. II. *Ann. Phys*. **1912**, 342, 657-699.
63. Zhang, J.; Wang, L.; Shao, Y.; Wang, Y. Q.; Gates, B. C.; Xiao, F. S. A Pd@Zeolite Catalyst for Nitroarene Hydrogenation with High Product Selectivity by Sterically Controlled Adsorption in the Zeolite Micropores. *Angew. Chem Int Ed*. **2017**, *56*, 9747-9751.

64. Zhao, M. T.; Yuan, K.; Wang, Y.; Li, G. D.; Guo, J.; Gu, L.; Hu, W. P.; Zhao, H. J.; Tang, Z. Y. Metal-organic frameworks as selectivity regulators for hydrogenation reactions. *Nature*. **2016**, *539*, 76-80.
65. Wu, B. H.; Huang, H. Q.; Yang, J.; Zheng, N. F.; Fu, G. Selective Hydrogenation of alpha, beta-Unsaturated Aldehydes Catalyzed by Amine-Capped Platinum-Cobalt Nanocrystals. *Angew. Chem Int Ed*. **2012**, *51*, 3440-3443.
66. Mao, J. J.; Chen, W. X.; Sun, W. M.; Chen, Z.; Pei, J. J.; He, D. S.; Lv, C. L.; Wang, D. S.; Li, Y. D. Rational Control of the Selectivity of a Ruthenium Catalyst for Hydrogenation of 4-Nitrostyrene by Strain Regulation. *Angew. Chem Int Ed*. **2017**, *56*, 11971-11975.
67. Armbrüster, M.; Schlogl, R.; Grin, Y. Intermetallic compounds in heterogeneous catalysis—a quickly developing field. *Sci. Technol. Adv. Mater.* **2014**, 15, 034803.
68. Studt, F.; Sharafutdinov, I.; Abild-Pedersen, F.; Elkjær, C. F.; Hummelshøj, J.S.; Dahl, S.; Chorkendorff, I.; Nørskov, J.K. Discovery of a Ni-Ga catalyst for carbon dioxide reduction to methanol. Discovery of a Ni-Ga catalyst for carbon dioxide reduction to methanol. *Nature Chem.* 2014, 6, 320–324.
69. S. Furukawa, S.; Komatsu, T. Intermetallic Compounds: Promising Inorganic Materials for Well-Structured and Electronically Modified Reaction Environments for Efficient Catalysis. *ACS Catal.* **2017**, 7, 735-765.
70. Armbrüster, M.; Kovnir, K.; Friedrich, M.; Teschner, D.; Wowsnick, G.; Hahne, M.; Gille, P.; Szentmiklosi, L.; Feuerbacher, M.; Heggen, M.; Girgsdies, F.; Rosenthal, D.; Schlogl, R.; Grin, Y. $Al_{13}Fe_4$ as a low-cost alternative for palladium in heterogeneous hydrogenation. *Nat. Mater*. **2012**, 11, 690– 693.
71. Maligal-Ganesh, R. V.; Xiao, C..; Goh, T. W.; Wang, L.-L.; Gustafson, J.; Pei, Y..; Qi, Z.; Johnson, D. D.; Zhang, S.; Tao, F.; W. Huang. A Ship-in-a-Bottle Strategy To Synthesize Encapsulated Intermetallic Nanoparticle Catalysts: Exemplified for Furfural Hydrogenation. *ACS Catal.* **2016**, 6, 3, 1754–1763.

TOC

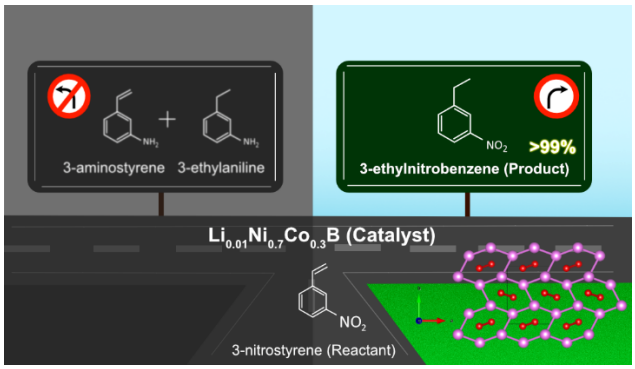
3-aminostyrene
3-ethylaniline
>99%
3-ethylnitrobenzene (Product)
Li0.01Ni0.7Co0.3B (Catalyst)
3-nitrostyrene (Reactant)